NASA-CR-201471

Structure and Dynamics of Coronal Plasmas

Grant NAGW-4081

Progress Report

For the period 1 July 1995 through 30 June 1996

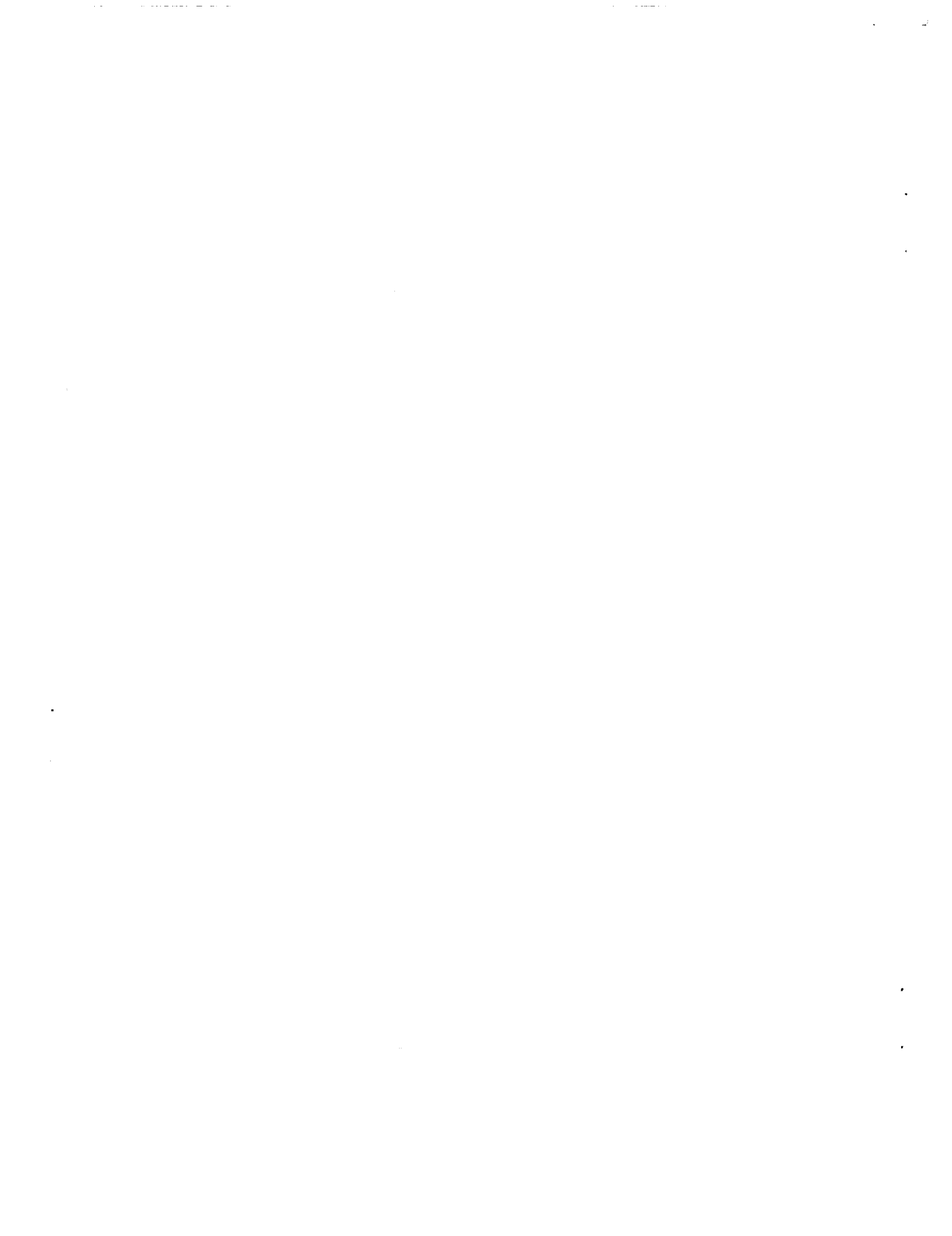Principal Investigator:

Dr. Leon Golub

July 1996

Prepared for

National Aeronautics and Space Administration

Washington, D. C. 20546

Smithsonian Institution
Astrophysical Observatory
Cambridge, MA 02138

The Smithsonian Astrophysical Observatory
is a member of the
Harvard-Smithsonian Center for Astrophysics

Progress Report

I. Work Completed During the Past Year:

During the past year this grant has funded research by Drs. Golub and DeLuca, graduate student A. Daw and undergraduates Ms. Wills and Mr. Hartl. The following is a brief summary of the published papers, abstracts and talks which have been supported by Grant NAGW-4081 within the present grant performance period.

1. The paper "Differential Magnetic Field Shear in an Active Region", by B. Schmieder, P. Demoulin, G. Aulanier and L. Golub, has been completed and has been accepted for publication in the Astrophysical Journal.

The three-dimensional extrapolation of magnetic field lines from a KPNO magnetogram alows us to understand the global structure of NOAA AR 6718, while Hα and x-ray observations allow us to compare various forms of magnetic field extrapolation to the observed AR structure.

Based on the fit between the observed and extrapolated structures we propose a differential magnetic field shear model for this active region. The decreasing shear in the outer (older) portions of the AR may indicate a continual relaxation of the magnetic field to a lower energy state as a function of time.

2. The paper "Observations and Modeling of the Solar Chromosphere Seen in Soft X-Ray Absorption by NIXT", by Daw, DeLuca and Golub, has been completed and has been accepted for publication in the Astrophysical Journal.

The Normal Incidence X-ray Telescope obtained a unique set of high resolution full disk solar images which were exposed simultaneously by X-rays in a passband at 63.5 Å and by visible light. The perfect alignment of a photospheric visible light image with a coronal X-ray image enables us to present observations of X-ray intensity vs an accurately determined height above the visible limb. The height at which the observed X-ray intensity peaks varies from 4000 km in active regions to 9000 km in quiet regions of the sun. The interpretation of the observations stems from the previously established fact that, for the coronal loops, emission in the NIXT bandpass peaks sharply just above the footpoints. Because there is not a sharp peak in the observed X-ray intensity vs off limb height, we conclude that the loop

footpoints, when viewed at the limb, are obscured by absorption in chromospheric material along the line of sight. We calculate the X-ray intensity vs height predicted by a number of different idealizations of the solar atmosphere, and we compare these calculations with the observed X-ray intensity vs height. The calculations use existing coronal and chromospheric models.

In order for the calculations to reproduce the observed off limb X-ray intensities, we are forced to assume an atmosphere in which the footpoints of coronal loops are interspersed along the line of sight with cooler chromospheric material extending to heights well above the loop footpoints. This means that coronal loop structures may be interpreted as isolated mini-atmospheres, with individual transition regions occurring at different heights, depending upon the coronal temperautre and density values. We argue that the absorption coefficient for NIXT X-rays by chromospheric material is roughly proportional to the neutral hydrogen density, and we estimate an average neutral hydrogen density and scale height implied by the data.

3. The paper "Modeling Magnetic Flux Emergence", by M. Wills and E. DeLuca was presented at the Solar Physics Division/AAS meeting in Madison in June 1996.

II. Plans for the Current Year:

Our plans for continuation of this work during the current year include i) projects which are under development and which are expected to lead to presentations, either in oral or written form, within the year, and ii) completion of the projects described above by submission of papers to refereed journals.

Among the projects which are under development at the present time, we mention the following:

1. "A Converging Flux Model for Point-Like Brightenings Around Sunspots". In collaboration with E. Priest and C. Parnell, we are analyzing coronal, chromospheric and photospheric data of intense x-ray brightenings in Moving Magnetic Features around sunspots. The work includes development of an MHD model for energy release by reconnection, consistent with the observed evolution of the photospheric field, and with the observed coronal energy release parameters.

2. "Difficulties in Observing Coronal Structure". This represents an invited keynote

Difficulties in Observing Coronal Structure

L. Golub
Smithsonian Astrophysical Observatory
60 Garden St., Cambridge Ma 02138

Abstract

There has developed in recent years a substantial body of evidence to indicate that the temperature and density structure of the corona are far more complicated than had previously been thought. We review some of the evidence and discuss some specific examples: observations of a limb flare, showing that the cool Hα material is *cospatial* with the hot x-ray emitting material; simultaneous NIXT and Yohkoh SXT observations of an active region, showing that loops seen in one instrument are not seen in the other, and that the effect works in *both* directions; comparisons of extrapolated magnetic field measurements to the observed coronal structure, indicating that neither potential nor constant-α force-free fits are adequate. We conclude with a description of two new instruments, the TRACE and the TXI, which will help to resolve some of these difficulties.

1 Overview

The importance of magnetic fields in determining the structure of the solar outer atmosphere has long been recognized. Billings (1966) [3] notes that magnetic fields "are employed, as a matter of fact, to explain all departures from a nonspherical [sic] distribution of matter in the corona, including the loop structure of the corona over active regions ..." Observations from sounding rockets in the late 60s and early 70s provided convincing evidence that loops structures, apparently outlining the magnetic field direction, are fundamental (Vaiana, Krieger & Timothy 1973) [28] and the *Skylab* observations in 1973–74 provided the impetus for constructing atmosphere models in which loop "mini-atmospheres" are the fundamental constituent of the inner corona (Rosner, Tucker & Vaiana 1978; Craig, McClymont & Underwood 1978) [18, 7].

This atmosphere is dynamic and constantly varying. Low (1990) [14] notes that the solar atmosphere is never truly quiescent or static, but adds that for the purpose of building models idealized static states may be used as an approximation to the physics underlying the apparent stability of long-lived structures. The extremely dynamic nature of the corona has been shown most effectively by the Soft X-ray Telescope (SXT) aboard the *Yohkoh* satellite: repeated transient loop brightenings in active regions (Shimizu *et al.* 1992) [23], continual rapid expansion outward of structures at the tops of active regions (Uchida *et al.* 1992) [26], jets of x-ray emission, apparently associated with reconnection events (Shibata *et al.* 1992) [22], among others.

paper for the STEPWG1 Workshop, "Measurements and Analysis of Solar 3D Magnetic Fields. The printed version will appear in a special issue of Solar Physics.

Thus, it is already clear that the simplest models of the corona – spherical or plane-parallel – are of limited applicability for interpreting the actual observations, and that the simplest loop atmosphere models – static loops – are also of limited usefulness. To these complications, we will add an additional set of worries, by showing that it is not at all clear that we are even now in a position to say that we know what coronal loops look like, or to know how the real corona is constructed of such loops.

2 Case Studies

In order to illustrate the difficulties alluded to in the Overview, we will examine five specific "case studies", each involving a seemingly reasonable question about the corona. The questions addressed by these studies are listed in Table 1, along with the answer to each question. The latter will be explained in the course of discussing each case. These examples are all taken from work related to flights of the Normal Incidence X-ray Telescope (NIXT) sounding rocket payload (Golub *et al.* 1990) [6] during the years 1989–1993.

Table 1: Observational questions about the solar corona.

Q1. Is the corona hot or cold at a given point in space?	A1. Depends on the viewing method.
Q2. Where is the "base" of the corona?	A2. Meaningful only for individual loops and probably unanswerable.
Q3. What is the transverse scale size of coronal structures?	A3. Our knowledge is limited by present instrumental resolutions.
Q4. What is the relation between the coronal B and x-ray emission?	A4. Data do not provide sufficient constraints.
Q5. What does the hot corona look like?	A5. Depends on the viewing method.

2.1 A limb flare

On 11 Sept. 1989, the NIXT rocket was launched at the start of a small flare (GOES classification C5). However, during the five-minute flight, a second flare began in an active region at the limb (Herant *et al.* 1991) [10]. Examination of the GOES x-ray light curves (Fig. 1) indicates that the limb flare began at about 16:36 UT during the decay phase of the larger on-disk flare. The NIXT observations also began at 16:36 UT, with the last image taken at 16:41:35 UT; the peak of the limb flare in x-rays is at $\approx$ 16:42 UT. Thus, the NIXT coverage could not have been better-timed.

Figure 2 shows simultaneous Hα and x-ray images of the flare at the time of the peak. The most striking aspect of this event seems to be the nearly identical size, shape and location of flare in the two wavelength regimes. This similarity is confirmed by a cross-correlation between the two datasets, shown in Fig. 3. The
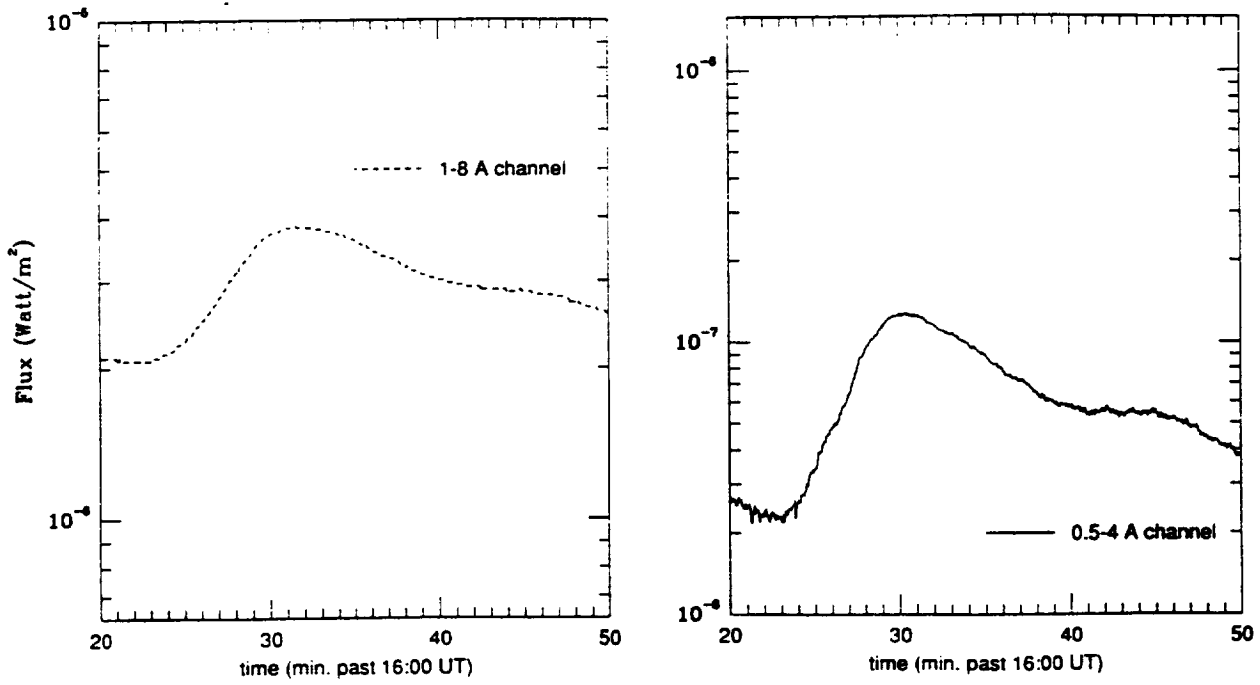
2

Figure 1: GOES 1-8 A and 0.5-4 A x-ray plots for 9/11/89.

contour lines show the x-ray brightness and the shaded region shows the Hα brightness: the two overlap to within the accuracy of alignment. Thus it would appear that the corona is both hot (x-ray) and cool (Hα) at the same place at the same time.

Figure 2: Simultaneous Hα and NIXT x-ray images of a limb flare.

Possible explanations exist, of course, for this apparent contradiciton. It is possible that the x-ray emission originates from a thin shell ahead of the advancing Hα region. Alternatively, hot and cool material may be intermingled on small spatial scales within the observed regions. The problem is not to come up with an answer, it is to come up with a *correct* answer.
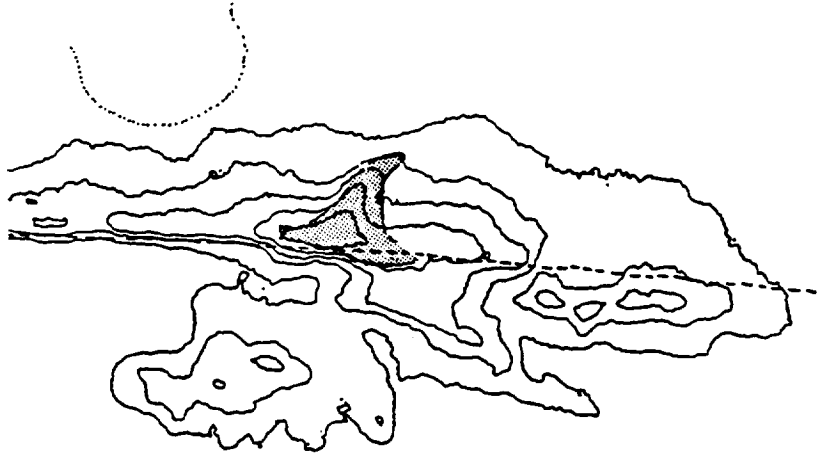
Figure 3: Relative positions of x-ray event and Hα material.

2.2 Simultaneous white light and x-ray imaging

Plane-parallel. or spherically symmetric models of the outer solar atmosphere treat the relation between temperature and height as one-dimensional. although not monotonic since the temperature at first increases with height but then decreases again. With the advent of loop model atmospheres. as described above. this fundamental view did not change in essence. but the temperature vs. height relation is transplanted into each loop instead of into the atmosphere as a whole. However, a flight of the NIXT payload on 22 February 1991 provided a unique dataset which shows that a more complicated geometry is required in order to explain the observations.

The multilayer mirrors used in the NIXT to provide x-ray imaging also reflect visible light with $\approx$ 50% reflectivity. In order to record only the (much fainter) x-ray image, two stages of visible-light rejection are employed: an entrance aperture filter, which cuts the visible to $\approx$ 1% and a focal plane filter, which provides 10^9 reduction in the visible. During the launch phase of the Feb. '91 flight, a portion of the entrance aperture filter broke. The instrument, however, was designed so that the focal plane filter acts as a back-up in the event of just such a failure. Thus, because the x-rays and the visible are reflected in the same way from the same mirror at the same time, we obtained simultaneous images of the visible disk and the corona. These are automatically coaligned and have the same plate scale, so that high precision (<one arcsecond) comparison between the two can be made.

Figure 4 shows a portion of the east limb from one of the exposures obtained on that flight. Note that there is a dark band at the limb, between the white light solar limb and the bright coronal x-ray emission. We note several features of this gap: 1.) it is most clearly evident when there is an x-ray emitting region behind the limb and no emitting region in front of the limb; 2.) the thickness of the gap varies between equator and poles, or between active regions and large scale "quiet" regions; 3.) at both the inner (white light) and outer (x-ray) heights, the gap is quite sharp. The question we will address is, how is this gap to be interpreted?
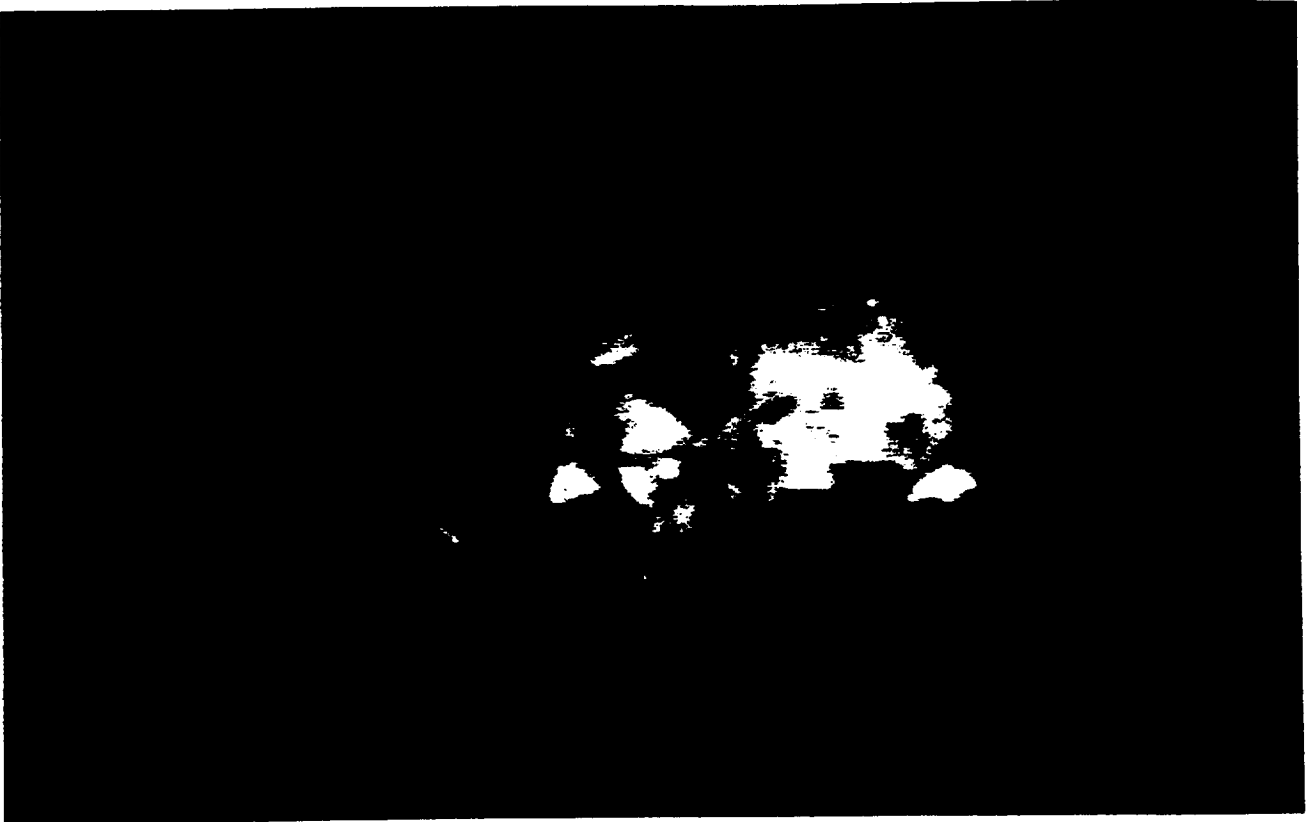
4

Figure 4: Portion of a combined NIXT/White Light image, showing a gap between the visible limb and the "base" of the corona. 22 Feb. 1991.

The data from this flight have been analyzed by Daw *et al.* (1995) [4], who find that a model in which the corona is viewed as consisting of a homogeneous set of loops, with temperature varying as a function of height in a uniform manner (Fig 5a) is not consistent with the data. In order to explain what is seen, it is necessary to use a model in which hot loops penetrate downward into an atmosphere having cool spicular material penetrating upward (Fig 5b). The two types of loops do not connect physically, but are interspersed along the line of sight. Thus, the gap is interpreted as the upward extent of spicular material, viewed along the line of sight at the limb and absorbing the x-rays emanating from loops *behind* the spicules.

We note that the soft x-rays in the NIXT data are strongly absorbed in spicular material, with about 10 arcsec path length required for 1/e absorption. The variation in thickness of the band indicates that spicules may extend farther in open field (e.g. coronal hole) regions than in higher temperature closed-loop regions, as reported by Huber *et al.* (1974) [12]. This interpretation of the NIXT data suggests that the footpoints of coronal loops cannot, in principle, be seen. When viewed at the limb, they are obscured by the intervening spicule material; when viewed from above, the projection angle is such that the height of the coronal "base" is very poorly determined. Depending upon the relative spatial density of hot vs. cool structures, there may be a small range of locations near the center of the disk which allow for both viewing the loops at an angle and for viewing them unobstructed. However, this is not yet known.
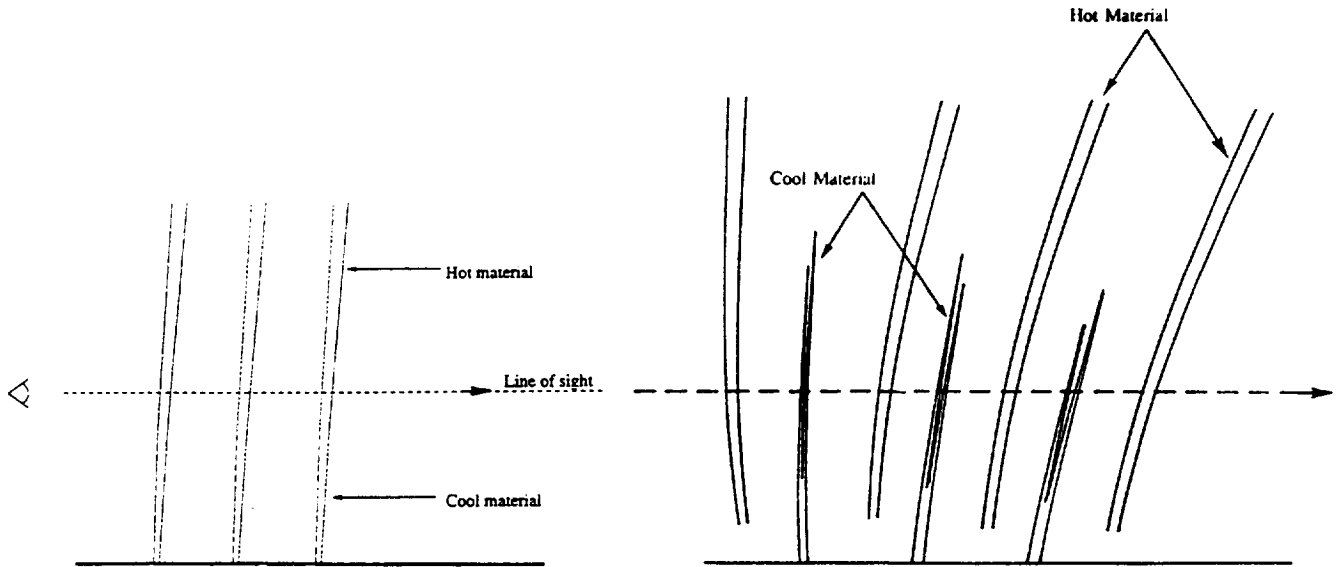
5

Figure 5: Two loop model atmospheres offering alternative explanations of the gap seen in Fig. 4. Modified plane-parallel model on left does not fit the data.

2.3 Active region fine structure

The progress in x-ray optics, when applied to solar coronal imaging, has consistently revealed coronal fine structure down to the resolution limit of the observing instruments (see, e.g. articles by Giacconi, Golub and Walker *et al.* in Linsky & Serio, 1993 [13]). An example is shown in Fig. 6, a coronal x-ray image from the NIXT instrument, obtained on 11 July 1991. There is clearly fine structure prevalent everywhere in the image and photographic analysis indicates that it reaches the combined limit set by the film and by the pointing stability of the rocket.

A quantitative analysis of the fine structure of several active regions observed by the NIXT was carried out by Gómez *et al.* (1993) [9]. By Fourier analyzing the images, they find a broad, isotropic power-law spectrum for the spatial distribution of soft x-ray intensities. The spectrum has a slope of $\alpha \approx -3$, which extends down to the resolution limit of the instrument at ≈ 0.75 arcsec.

A similar result has been obtained by Martens & Gómez (1992) [15] from analysis of *Yohkoh* SXT data: the Fourier transform distribution is a power-law (with somewhat smaller slope of $\alpha \approx -2.4$) which extends down to the Nyquist frequency. Thus, for both cases in which the procedure has been carried out, the spatial structuring of the corona is seen to be limited by the resolution of the imaging instrument. The implication, since the sun does not know what instrument we are using to observe it, is that we have not yet fully resolved the coronal fine structure. Thus, the answer to Question 3, "What is the transverse scale size of coronal structures?", is that we do not yet know.

6

Figure 6: 11 July 1991 NIXT image.

2.4 Magnetic field extrapolation vs. observed structure

There have been only a limited number of attempts in recent years to carry out direct comparisons between high resolution coronal observations and magnetic field extrapolations. if we exclude attempts to explain the onset of flares by testing the non-potentiality of fields. For non-flaring regions. i.e. normal coronal structure. Poletto *et al.* (1975) [17] and Sakurai & Uchida (1977) [19] had reasonable success at the level of late 60s and early 70s resolution. More recently Sams *et al.* (1992) [20] found a general agreement between extrapolations and the structures seen in the NIXT. although close examination shows that the agreement is quite poor in detail. Metcalf *et al.* (1994) [16] conclude. from comparison of vector magnetograph data (giving the locations of vertical currents) with Yohkoh SXT coronal data. that there is a very por spatial and temporal correlation between the locations of the currents and the locations of bright coronal structures.

In a recent study. Schmieder *et al.* (1996) [21] have used high resolution NIXT data combined with Kitt Peak magnetogram and Multi-channel Double Pass (MSDP) spectrograph data. to study in more detail the relationship between the observed structure and the type of magnetic field extrapolation employed. The extrapolation code is based on the work of Alissandrakis (1981) [1] as modified by Démoulin *al.* (1996) [5]. A single active region. AR 6718 on 11 July 1991. was chosen for study: an x-ray image of the reigon and the corresponding portion of the magnetogram are shown in Fig. 7.
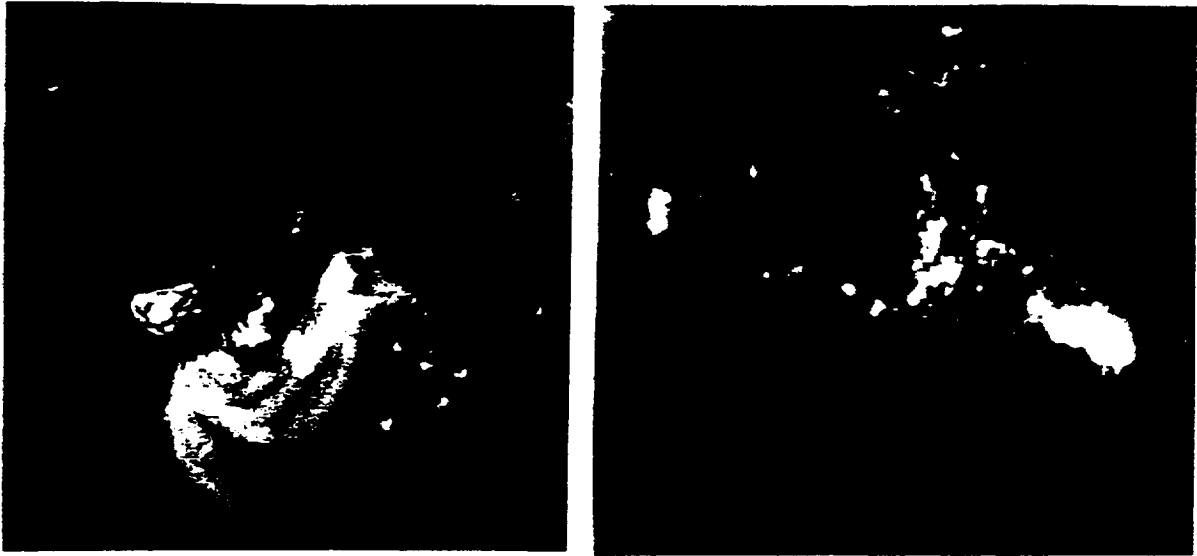
Figure 7: NIXT x-ray image of AR 6718 and KPNO magnetogram of the region.

The first result is that a potential-field extrapolation does not represent the observed coronal structure at all, and that even a constant-α force-free field extrapolation is not adequate. Fig. 8 shows extrapolations using three values of α. The left-most panel shows $\alpha = 0$, i.e. a potential field. Note that the connectivity of the field lines is entirely different from that of the observed strcutres. The two force-free fits in the middle and right-hand panels match portion of the region, but neither one in itself is a good fit. What we find is that the inner portion of the active region is well matched by the larger value of α while the outer portion of the region is matched by a lower α.

A possible interpretation of this result is that there is, with time, a relaxation of the magnetic field, as proposed by Heyvaerts & Priest (1984) [11]. In a highly-conducting plasma, small-scale processes dissipate magnetic energy much more rapidly than helicity $H \equiv \int \mathbf{A} \cdot \mathbf{B}\, dV$ (Taylor, 1974; Berger, 1985) [25, 2]. With this constraint the magnetic field does not relax to a potential state, but to a linear force-free state. The gradient of α found in this region may be indicative of this ongoing relaxation process.

2.5 Yohkoh SXT vs. NIXT comparison

In April 1993 the Yohkoh SXT carried out a special observing sequence simultaneous with a flight of the NIXT rocket. An inital comparison of the two datasets was carried out by Yoshida *et al.* (1995) [27] for a quiet corona region. Because the SXT temperature response is somewhat harder than that of the NIXT (> 2.5 MK for SXT vs. $1 - 3$ MK for NIXT) it was expected that the SXT would see the hotteer top portions of coronal loops while the NIXT would see the lower portions or the footpoints. This was indeed generally seen to be the case in that study.
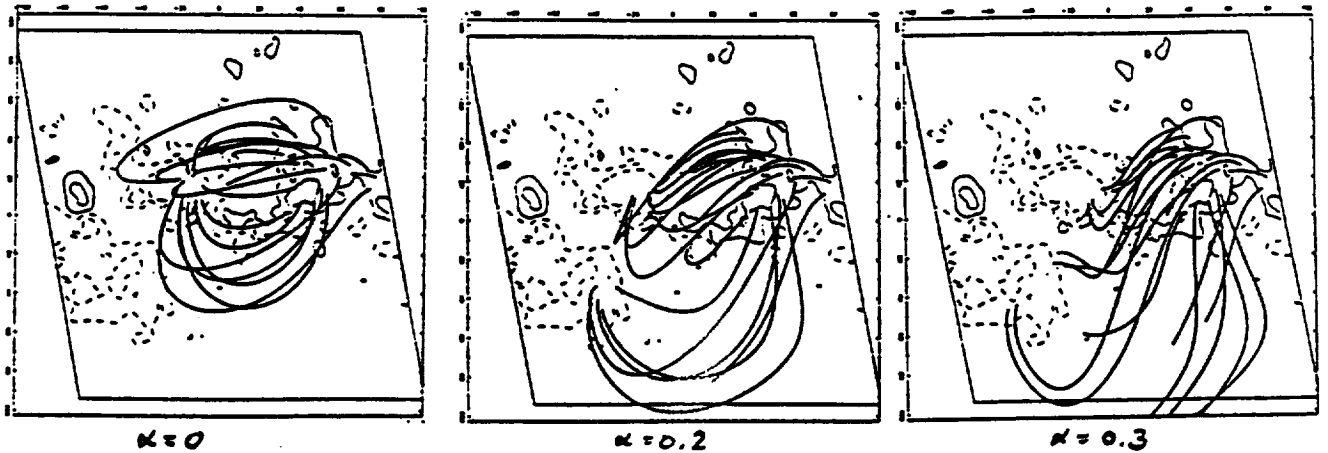
8

Figure 8: Magnetic field extrapolations of AR 6718, with three values of α.

However, subsequent evaluation of the one active region on the disk on that day is showing a completely different and unexpected result. One expects that "all x-ray images are alike", so that the two should show toughly similar structures. Viewed from a distance, the two observations seem to be showing the same coronal features. However, detailed examination shows some remarkable discrepancies between the two.

Fig. 9 shows the comparison of NIXT and Yohkoh SXT observations, with arrows pointing to three locations in the region. These are places where a structure or set of structures is visible in one of the images and *entirely invisible* in the other; the effect works both ways. Thus, if only one of these images were available, we would draw reonneous conclusions about the coronal structure, since there would be no indication at all that some structures are present.

The seriousness of this problem is obvious: if we intend to study the formation, stability and dynamics of coronal structures, one must first be able to see them. A partial solution to this problem is described in the next section.

3   Some Partial Solutions

The above discussion provides only a partial listing of some of the problems we are encountering in attempting to study the formation, heating, structuring and dynamics of the solar corona. In this section we describe two new instruments which will help to solve, or at least advance, some of these problem areas. The TRACE instrument will have the highest spatial resolution ever used to observe the corona, as well as the ability to discriminate multiple temperature regimes and to view the atmosphere from the upper chromosphere up into the active region corona. The TXI is a rocket-borne payload which will have the capability of observing the entire sequence of successive ionization stages of a single element from $< 10^6$ K to $> 3 \times 10^6$ K, and will also determine flow velocities at these temperatures.
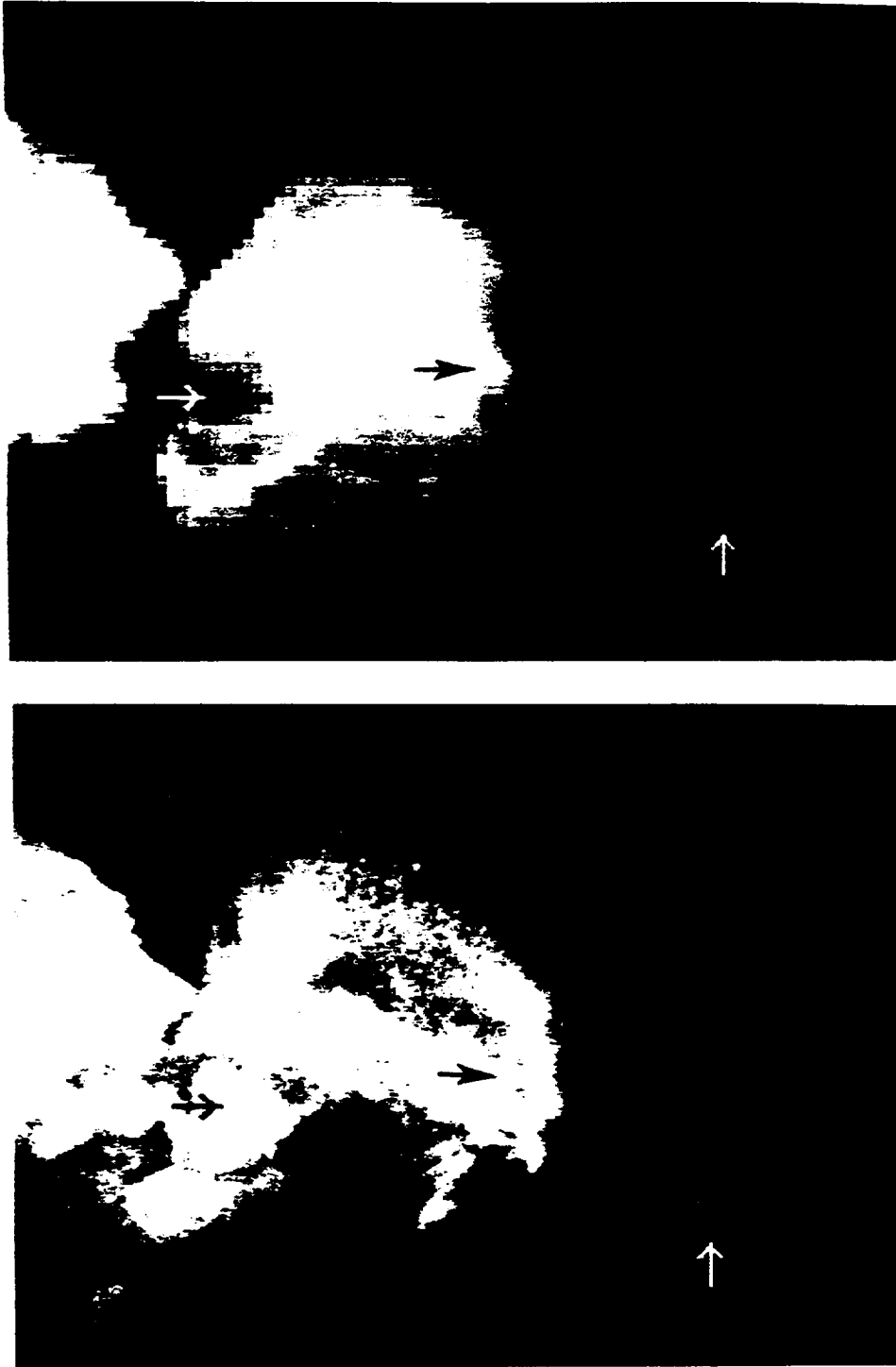
9

Figure 9: Comparison between Yohkoh SXT (top) and NIXT (bottom) observations of an active region: arrows indicate structures seen in one of the instruments but *not* seen in the other.

Table 2: TRACE spectral regions & observing parameters.

Central Wavelength (Å)	Width (Å)	Ion	Location
2500	Broad	Continuum	Photosphere
1700	"	T_{min}/Chrom.	
1570	30	C I, Fe II, Cont.	"
1550	30	C IV	Transition Region
1216	84	H Ly α	Chromosphere
284	14	Fe XV	Corona
195	10	Fe XII	"
		(+Fe XXIV)	Flares
171	9	Fe IX	Corona

3.1 TRACE

The Transition Region And Coronal Explorer (TRACE) is designed to quantitatively explore the connections between fine-scale magnetic fields at the solar surface and the associated plasma structures in the solar outer atmosphere. The TRACE instrument uses multiple UV and normal-incidence XUV channels to collect images of atmospheric plasma from 10^4 K to 10^7 K. Many of the physical problems that arise in this portion of the atmosphere – plasma confinement, reconnection, wave propagation, plasma heating – arise throughout space physics and much of astrophysics as well. Although recent pogress in, e.g., numerical MHD simulations has been substantial (viz. Low 1990), use of these models requires close guidance by the observations, because the enormous range in parameter scale sizes cannot be realized in the computations.

The telescope provides true one arcsecond resolution (1 pixel is 0.5 arcsec) and temporal resolution as short as a fraction of a second for bright sources. Table 2 lists the operating spectral bands, the associated temperatures and the portions of the atmosphere covered. The instrument uses four normal incidence coatings, one for broadband UV and three for narrowband XUV operation. The UV channel includes a set of narrowband filters at the focal plane, thereby allowing sub-channels which detect portions of the atmosphere from the photosphere to the transition region. Selection of the XUV channels is based on a thorough analysis carried out by Golub, Hartquist & Quillen (1989), who analyzed the spectral region accessible to normal incidence techniques and determined the best lines to use for particular atmospheric features of interest.

TRACE is launched on a Pegasus-XL into a polar, sun-synchronous orbit, thereby providing continuous observation of the sun. Continuous observing for about 8 months is planned over a 1-year baseline mission. TRACE produces data complementary with SOHO, and planning of the TRACE daily observations is being coordinated with those of SOHO.

The main components of the TRACE instrument are shown in Fig. 10. The TRACE instrument consists of a 30 cm diameter Cassegrain telescope and a fil-
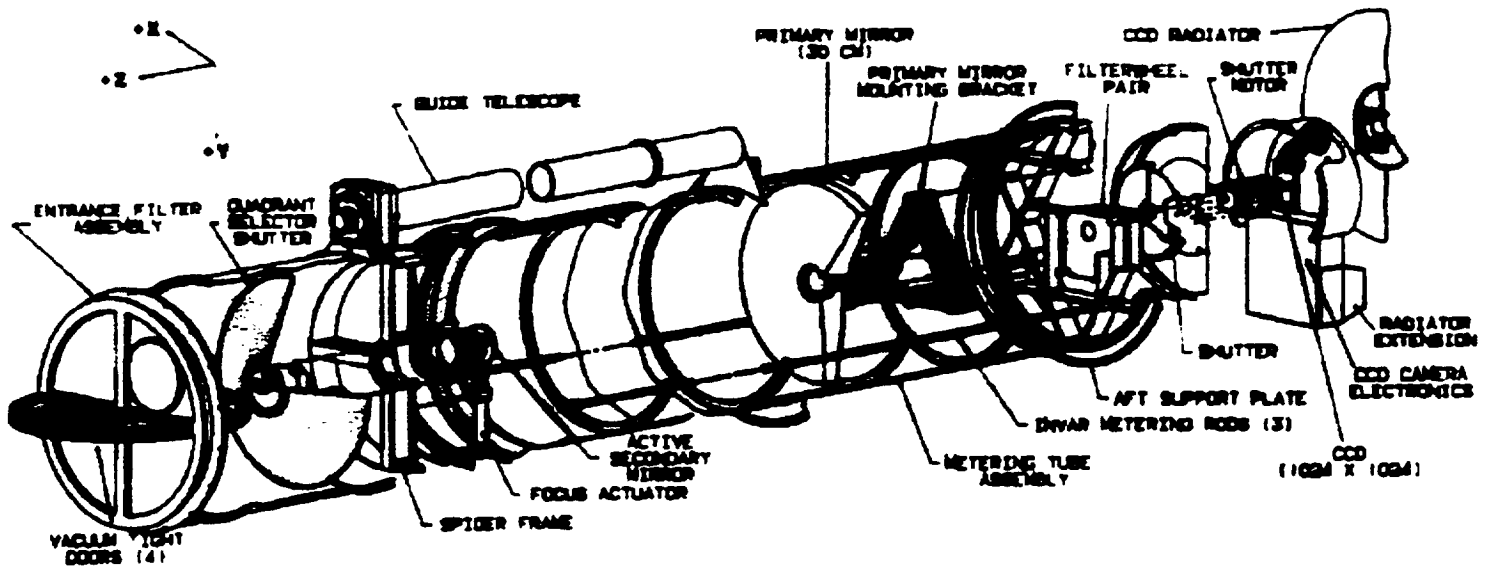
Figure 10: Major system components of the TRACE instrument.

ter system feeding a CCD detector. Each quadrant of the telescope is coated for sensitivity to a different wavelength range. Light entering the instrument passes first through an entrance filter assembly which transmits only UV and soft x-ray radiation, thus blocking the solar heat from reaching the mirrors. A large rotating quadrant shutter selects one quadrant at a time for viewing. The secondary mirror of the telescope is active, to correct for pointing jitter to better than 0.1 arcsec.

The converging beam from the secondary mirror passes through the central hole in the primary, where it encounters two filter wheels in series, each having three filters and one open position. These wheels contain both the XUV light-blocking and the UV passband filters. Finally, there is a focal plane shutter and a 1024X1024 CCD, for a field of view of 8.5X8.5 arcmin. Mosaic observations are planned, for larger field and daily full disk data-taking. The TRACE launch is late in 1997, and mission lifetime is at least 8 months. Thus it will be observing during the rise phase of the new solar cycle.

Some of the scientific objectives of the mission are:

- Magnetic Field Structure and Evolution.
- Coronal Heating and Magnetic Fields.
- Onset of Coronal Mass Ejections.
- Variability of X-ray Bright Points.

The mission and its objectives are described in more detail in Tarbell *et al.* (1994).

3.2 TXI

The Tuneable X-ray Imager (TXI) is a high resolution coronal imaging instrument which has the ability to produce near-monochromatic images tuneable over a range of XUV wavelengths. The present design covers the wavelength range 170 – 220 Å, which includes the strong series of iron lines from Fe IX through Fe XIV, inclu-
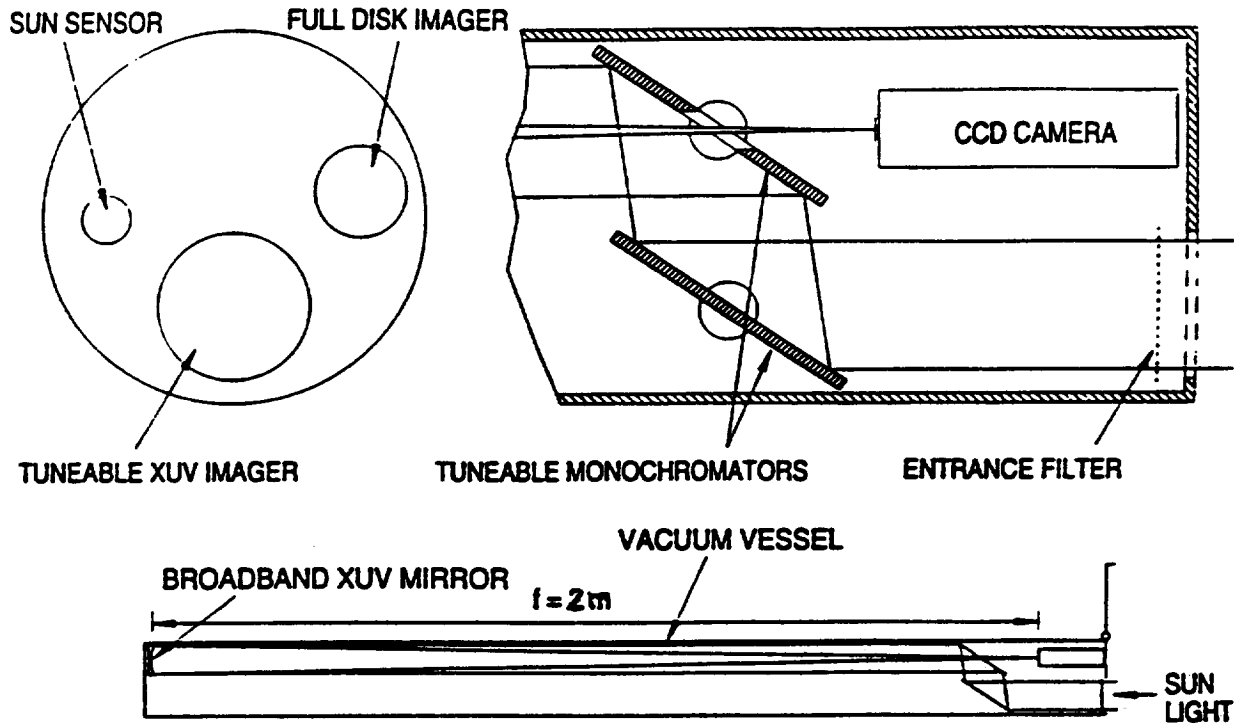
12

Figure 11: Schematic layout of the Tuneable XUV Imager.

sive. Thus, the problem of "missing" structures is solved, for the temperature range $\log T = 5.8 - 6.4$, because *all* of the successive ionization stages are isolated and recorded.

Figure 11 shows a schematic layout of the instrument. Spectral isolation is achieved by using a double-crystal monochromator, which feeds a broadband telescope, coated with an XUV multilayer having $\Delta\lambda \sim 30$ Å(FWHM). The monochromator is made as narrowband as possible, which in this instance is ≈ 4 Å, and it is tuned by rotating the two plane mirrors in parallel. A Cowan-Golovchenko arrangement is used (Cowan 1983), which has the highly desireable property that the entrance and exits beams stay fixed during tuning. Thus, there is no image motion in the focal plane as the wavelength is changed.

Table 3.2 shows the strongest lines in the TXI passband. Depending upon line strength and available exposure time, it appears possible to record data out to $\approx$ 220 Å; no data below 170 Å are recorded because aluminum light-blocking filters are used at the entrance aperture and at the focal plane. We note that line multiplets, such as Fe XII near 193 Å, do not smear the image, because this is a non-dispersive system.

The TXI sounding rocket program has just received approval from NASA to begin construction (May 1996). Present plans are to have the payload ready to fly in two years, by the summer of 1998. A summer launch is necessary in order to reduce absorption by the residual even at rocket altitudes. A minimum altitude of 100 miles is necessary for the wavelengths observed in this experiment, and a line-of-sight to the sun as near normal to the plane of the atmosphere as possible is required. The launch therefore takes place around local noon in White Sands, NM.

13

Table 1. Strongest lines in the TXI passband.

Ion	Wavelength (Å)	log T
Fe IX	171.08	6.0
O V	172.17	5.4
O VI	172.94	5.5
	173.08	
Fe X	174.53	6.1
	177.24	
Fe XI	180.42	6.2
Si XI/Fe XII	186.88	6.2
Fe XI	188.22	6.2
Fe XXIV	192.03	7.3
Fe XII	192.40	6.2
	193.52	
	195.13	
Fe XIII	202.04	6.2
	203.82	
Fe XIV	211.32	6.3
He II	237.35	4.7

3.3 The Solar Radio Telescope

Of course, it is not only in the area of space-based instrumentation that solutions to the present set of problems in solar physics may be sought. In this section we describe a representative ground-based instrument, designed to map the magnetic field structure and topology in the corona.

A proposal for a dedicated Solar Radio Telescope which represents a major advance on current radio facilities is currently being explored (a report by D. Gary and T. Bastian will be available shortly). The ability to map solar magnetic fields above coronal active regions is one of the major goals of this telescope. The features necessary to carry out such a goal are:

• the ability to make radio images of active regions on short timescales with high spatial resolution and high dynamic range;

• the ability to make images at many closely-spaced frequencies across a broad frequency range nearly simultaneously; and

• accurate polarimetry.

The proposed instrument which provides these features consists of an array which contains many small dishes (presently planned to be 40) with full-disk coverage, three large ($\sim$ 25 m) dishes to provide sensitivity and allow accurate calibration, and receivers which incorporate the frequency-agile characteristics so successfully demonstrated by the OVRO array with a target range from 300 MHz to 30 GHz. This instrument would have 2.5 times as many baselines as the VLA, and requires a

large correlator to handle them. Recent advances in broadband microwave components, large correlators and computers make such an instrument possible for a low cost. Considerable effort will also be expended on software for real-time processing of the data into a form (images and coronal field maps) suitable for immediate use by the broader solar community.

3.3.1 Vector magnetic fields

Finally, we mention the almost obvious point that vector magnetograms are crucially important in the comparison between surface fields and coronal structure/stability. Ground-based observations have progressed enormously, but there still remains the basic question: how much of the observed variability is due to atmospheric effects and how much is intrinsic to the source? This question has been answered in part by comparing observations taken simultaneously at widely-separated sites. However, the best way to answer the question and to obtain the highest quality observations, is to place a vector magnetograph in orbit.

References

[1] Alissandrakis, C.E. 1981. *Astron. & Astrophys.* **100**, 197.

[2] Berger, M.A. 1985. *Astrophys. J. Suppl.* **59**, 433.

[3] Billings, D.E. 1966. *A Guide to the Solar Corona*, Academic Press, New York.

[4] Daw, A., DeLuca, E. and Golub, L. 1995. *Astrophys. J.* **453**, 929.

[5] Démoulin, P., Balalá, L.G., Mandrini, C.H., Hénoux, J.C. and Rovira, M.G. 1996. *Astron. & Astrophys.* (in press).

[6] Golub, L., Herant, M., Kalata, K., Lovas, S., Nystrom, G., Pardo, F., Spiller, E. and Wilczynski, J. 1990. *Nature*, No. 6269, 842.

[7] Craig, I.J.D., McClymont, A.N. and Underwood, J.H. 1978. *Astron. & Astrophys.* **70**, 1.

[8] Golub, L., Hartquist, T.W. and Quillen, A.C. 1989. *Sol. Phys.* **122**, 245.

[9] Gómez, D.O., Martens, P.C.H. and Golub, L. 1993. *Astrophys. J.*, **405**, 767.

[10] Herant, M., Pardo, F., Spiller, E. and Golub, L. 1991. *Astrophys. J.* **376**, 797.

[11] Heyvaerts, J. and Priest, E.R. 1984. *Astrophys. J.* **137**, 63.

[12] Huber, M.C.E., Foukal, P.V., Noyes, R.W., Reeves, E.M., Schmahl, E.J., Timothy, J.G., Vernazza, J.E. and Withbroe, G.L. 1974. *Astrophys. J. (Letters)* **194**, L115.

[13] Linsky, J.F. and Serio, S., eds. 1993. *Physics of Solar and Stellar Coronae*, Kluwer Academic Publishers, Dordrecht, Holland.

[14] Low, B.C. 1990. *Ann. Rev. Astron. Astropjhys.* **28**, 491.

[15] Martens, P.C.H. and Gómez, D.O. 1992. *Publ. Astronom. Soc. Japan*, **44**, L187.

[16] Metcalf, T.R., Canfield, R.C., Hudson, H.S., Mickey, D.L., Wülser, J.P., Martens, P.C. and Tsuneta, S. 1994. *Astrophys. J.*, **428**, 860.

[17] Poletto, G., Vaiana, G.S., Zombeck, M.V., Krieger, A.S. and Timothy, A.F. 1975. *Sol. Phys.* **44**, 83.

[18] Rosner, R., Tucker, W.H. and Vaiana, G.S. 1978. *Astrophys. J.*, **220**, 643.

[19] Sakurai, T. and Uchida, Y. 1977. *Sol. Phys.* **52**, 397.

[20] Sams, B.J., III, Golub, L. and Weiss, N.O. 1993. *Astrophys. J.*, **399**, 313.

[21] Schmieder, B., Démoulin, P., Aulanier, G. and Golub, L. 1996. *Astrophys. J.* (in press).

[22] Shibata, K., *et al.* 1992. *Publ. Astronom. Soc. Japan*, **44**, L173.

[23] Shimizu, T., Tsuneta, S., Acton, L.W., Lemen, J.R., and Uchida, Y. 1992. *Publ. Astronom. Soc. Japan*, **44**, L147.

[24] Tarbell, T.D., Bruner, M., Jurcevich, B., Lemen, J., Strong, K., Title, A., Wolfson, J., Golub, L. and Fisher, R. 1994. Proc. of the 3rd SOHO Workshop, ESA SP-373, Dec. 1994.

[25] Taylor, J.B. 1974. *Phys. Rev. Lett.* **33**, 1139.

[26] Uchida, Y., McAllister, A., Strong, K.T., Ogawara, Y., Shimizu, T., Matsumoto, R., and Hudson, H.S. 1992. *Publ. Astronom. Soc. Japan*, **44**, L155.

[27] Yoshida, T., Tsuneta, S., Golub, L., Strong, K. and Ogawara, Y. 1995. *Publ. Astron. Soc. Japan* **47**, L15.

[28] Vaiana, G.S., Krieger, A.S. and Timothy, A.F. 1973. *Sol. Phys.* **32**, 81.

16